Geophysical Research Letters

RESEARCH LETTER
10.1029/2021GL092748

Key Points:

- The excessive atmospheric blockings over East Siberia enhanced the Meiyu-Baiu rainfall in June–July 2020
- The low Arctic sea ice favored East Siberian blockings and greatly intensified the Meiyu-Baiu rain belt, especially in July 2020

Correspondence to:
A. Dai,
adai@albany.edu

Citation:
Chen, X., Dai, A., Wen, Z., & Song, Y. (2021). Contributions of Arctic sea-ice loss and East Siberian atmospheric blocking to 2020 record-breaking Meiyu-Baiu rainfall. *Geophysical Research Letters*, *48*, e2021GL092748. https://doi.org/10.1029/2021GL092748

Received 4 FEB 2021
Accepted 10 APR 2021

Contributions of Arctic Sea-Ice Loss and East Siberian Atmospheric Blocking to 2020 Record-Breaking Meiyu-Baiu Rainfall

Xiaodan Chen[1], Aiguo Dai[2], Zhiping Wen[1,3], and Yuanyuan Song[4]

[1]Department of Atmospheric and Oceanic Sciences & Institute of Atmospheric Sciences, Fudan University, Shanghai, China, [2]Department of Atmospheric and Environmental Sciences, University at Albany, SUNY, Albany, NY, USA, [3]Innovation Center of Ocean and Atmosphere System, Zhuhai Fudan Innovation Research Institute, Zhuhai, China, [4]CAS Key Laboratory of Regional Climate-Environment for Temperate East Asia, Institute of Atmospheric Physics, Chinese Academy of Sciences, and University of Chinese Academy of Sciences, Beijing, China

Abstract Heavy Meiyu-Baiu rainfall occurred over central-east China and Japan in June–July 2020. This study analyzes observational and reanalysis data and performs atmospheric model simulations to investigate its causes. It is found that low Arctic sea ice cover (SIC) in late spring-early summer of 2020 along the Siberian coast was an important factor. The low SIC caused local warming and high pressure, resulted in excessive atmospheric blockings over East Siberia, which caused cold air outbreaks into the Meiyu-Baiu region, stopped the seasonal northward march of the Meiyu-Baiu front, and increased the thermal contrast across the front, leading to record-breaking rainfall in June–July 2020. Our results suggest that the 2020 extreme Meiyu-Baiu was partly caused by the low SIC around the Siberian coast through its impact on East Siberian blockings. As sea ice along the Siberian coast decreases under global warming, its variations and thus influence on Meiyu-Baiu rainfall may weaken.

Plain Language Summary Meiyu-Baiu, a west—east oriented stationary front from central-east China to Japan, usually persists from mid-June to mid-July. In June–July 2020, central-east China and Japan encountered record-breaking Meiyu-Baiu rainfall. Through analyses of observational and reanalysis data, we found that excessive East Siberian atmospheric blockings—large-scale quasi-stationary anticyclonic circulations—during the 2020 Meiyu-Baiu season increased cold air outbreaks into the Meiyu-Baiu region, stopped the northward march of the Meiyu-Baiu front, and enhanced the temperature contrast across the front, leading to record-breaking Meiyu-Baiu rainfall in 2020. Using atmospheric model experiments, we further show that the frequent East Siberian blockings can be largely attributed to excessive sea ice melting and the concurring warming along the Siberian coast. The lower-atmospheric warming reduced local meridional temperature gradients and zonal winds, which favors East Siberian blockings. Our results highlight the effect of Arctic sea ice decline and the associated warming on Meiyu-Baiu rainfall and provide a new mechanism for the Arctic to affect mid-latitude precipitation in late spring-early summer. This Arctic effect may change in the future as late spring-early summer sea ice diminishes under global warming.

1. Introduction

From mid-June to mid-July, a southward surge of cold air from high latitudes prevents the Asian summer monsoon from advancing further northward, generating a quasi-stationary west-east oriented front from central-east China to Japan (Ding, 1991; Tao & Chen, 1987; Zhu et al., 2003). The resultant persistent rainfall is referred to as the Meiyu in China, Changma in Korea, and Baiu in Japan. In June–July 2020, extremely heavy Meiyu-Baiu rainfall hits Japan and the middle-lower reaches of the Yangtze River in China, generating record-breaking accumulated rainfall and severe floods.

Previous studies suggest that East Asian precipitation in early summer can be influenced by many factors, such as tropical and North Pacific Ocean temperatures (Ren et al., 2013), Indian Ocean temperatures (Kosaka et al., 2013), atmospheric teleconnections (Zhang et al., 2021), and snow cover over the Tibetan Plateau and Siberia (Yim et al., 2010; Xiao & Duan, 2016). Prominent factors that enhance Meiyu-Baiu rainfall include an El Niño in preceding winter (Huang & Wu, 1989; Wu et al., 2003), a warm Indian Ocean (Zhang

et al., 2017; Zhou et al., 2021), and a warm phase of the Pacific decadal Oscillation (PDO, Si et al., 2009; Zhu et al., 2015). These factors can modulate the Pacific subtropic high and the northward moisture flux into the Meiyu-Baiu region. However, for the 2020 extreme Meiyu-Baiu rainfall, neither a preceding El Niño nor strong simultaneous warming in the Indian Ocean appeared (WMO, 2020; Takaya et al., 2020), and the PDO is at a neutral phase (https://www.ncdc.noaa.gov/teleconnections/pdo/). Thus, previously noticed factors cannot fully explain the heavy 2020 Meiyu-Baiu rainfall.

A recent study found that the warm Indian Ocean can help explain the enhanced Meiyu-Baiu rainfall only for June but not July of 2020 (Zhou et al., 2021). Takaya et al. (2020) estimated that the warm Indian Ocean contributed about one fourth to the 2020 Meiyu-Baiu rainfall anomaly and suggested that extratropical forcing is essential for explaining the rest. Liu et al. (2020) found that the phase transition of the North Atlantic Oscillation (NAO) influenced the 2020 Meiyu-Baiu front, which also implies an important role of mid-to-high latitude atmospheric circulation. Previous studies suggested that the mid-high latitude atmospheric circulation, especially Eurasian atmospheric blocking, is vital in prolonging the Meiyu-Baiu season and increasing its rainfall intensity and accumulated amount (e.g., Chen et al., 2007; Chen and Zhai, 2014; Li et al., 2001; Li et al., 2018; Ninomiya & Shibagaki, 2007; Park & Ahn, 2014; Wang, 1992).

On the other hand, observational and modeling studies found that winter Arctic sea ice cover (SIC) can influence the frequency and persistence of Eurasian blocking (e.g., Chen et al., 2020; Luo & Zhang, 2020; Luo et al., 2019; Mori et al., 2014; Ruggieri et al., 2016; Yao et al., 2017). In the late spring-early summer of 2020, Arctic sea ice extent was at the lowest levels since 1979 due to a Russian heat wave persisting from January to May in 2020 (NSIDC, 2020) that resulted from a combination of internal variability and anthropogenic influences (Overland & Wang, 2020; WWA, 2020). Whether and how the low Arctic SIC is linked to the Eurasian atmospheric blocking and thus the Meiyu-Baiu rainfall in 2020 is unclear.

In this study, we examine the East Siberian blocking anomaly during the 2020 Meiyu-Baiu period, explore its effect on the Meiyu-Baiu rainfall, and investigate its link to the record-breaking Arctic sea ice melting using reanalysis data and atmospheric model experiments.

2. Data, Methods, and Experiments

Daily data on a 1° lon/lat grid from January 1979–July 2020 for horizontal winds, geopotential height, air temperature, precipitation, SIC, sea surface temperature (SST), surface sensible and latent heat fluxes, surface longwave and shortwave radiation fluxes were obtained from ERA5 reanalysis (Hersbach et al., 2020). We evaluate ERA5 precipitation with a precipitation data set on a 0.05° lon/lat grid provided by the National Meteorological Information Center in China, which combines raingauge measurements with precipitation estimates from radar and satellite sensors (Pan et al., 2015). The ERA5 precipitation captures the spatial distribution and temporal evolution of the Meiyu-Baiu rainfall from June 1st to July 31st in 2020 (Figures 1a and 1b). The daily evolutions of the domain-averaged rainfall in observation and ERA5 are highly correlated ($r = 0.75$; Figure 1b).

We used a two-dimensional blocking index proposed by Dunn-Sigouin et al. (2013) to quantify atmospheric blockings. First, the standard deviation (STD) of daily 500-hPa geopotential height (Z500) anomalies north of 30°N is calculated. An instantaneous blocking is identified over the area that is within the closed contour of 1.5 Z500 STDs and extends over 2.5×10^6 km^2 or more. A reversal of the Z500 meridional gradient on the equatorward flank of the instantaneous blocking is required. Instantaneous daily blockings in two successive days are considered as one blocking event if their spatial overlap is greater than 50%; otherwise, they belong to different blocking events. A blocking event lasting for at least 3 days over East Siberia (90°E–180°, 60°–85°N) is defined as an East Siberian blocking event. We calculated the 1979–2019 climatology for the blocking frequency and other variables for each calendar day, and the anomaly is relative to this daily climatology.

We conducted atmospheric modeling experiments using the Community Atmosphere Model version 6 (CAM6) in the Community Earth System Model, version 2 (CESM2, Danabasoglu et al., 2020). The CAM6 was run with 1.25°lon × 0.9°lat horizontal spacing, 32 vertical levels from the surface to 2.26-hPa. In the control experiment (CTL), 1995–2005 monthly climatological SST and SIC were used as the lower boundary

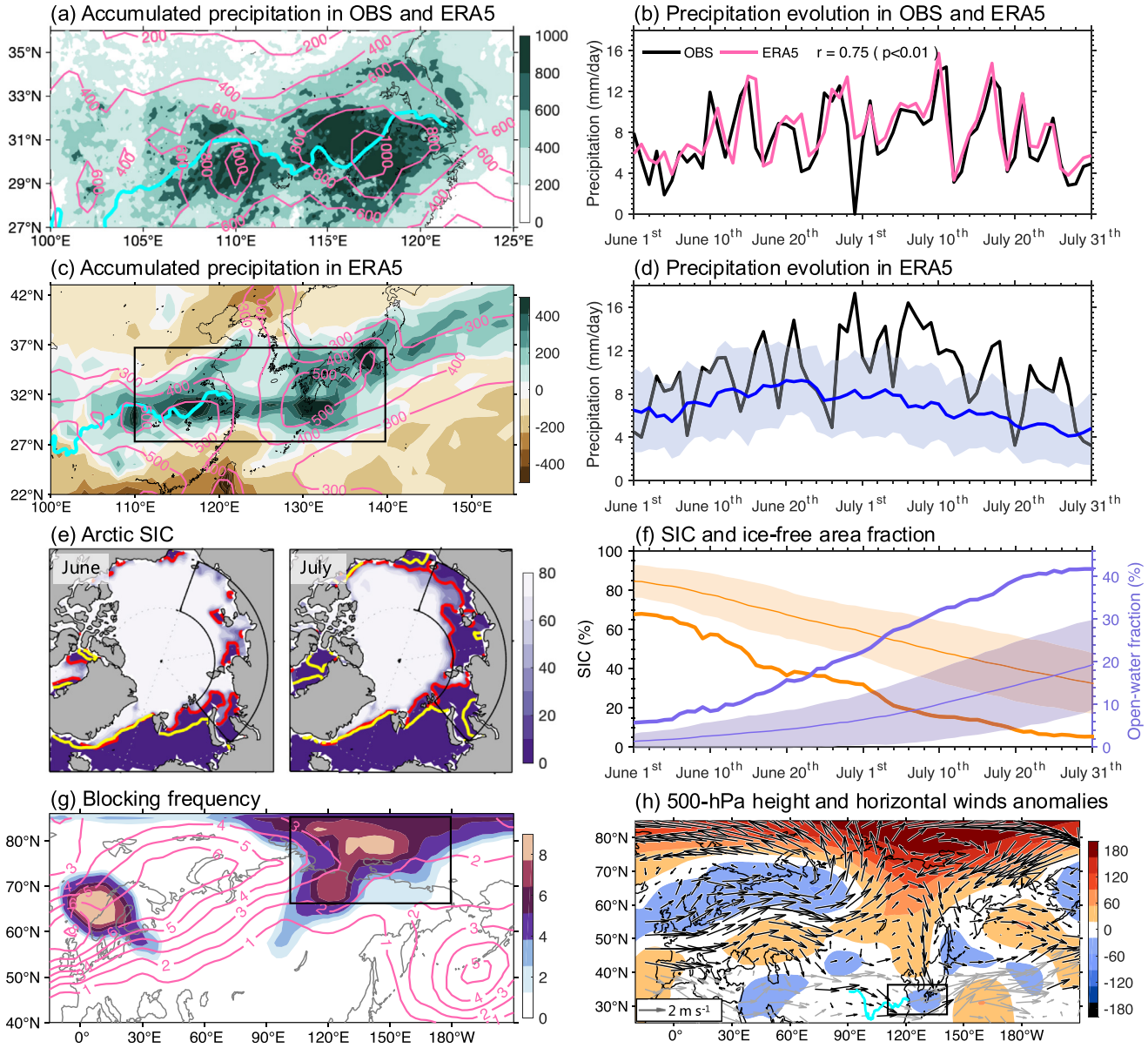

Figure 1. Precipitation, Arctic sea ice, and atmospheric circulation conditions in early summer 2020. (a) Observed (shading) and ERA5 (contours) precipitation (mm) accumulated from June 1st to July 31st. (b) Time series of observed (black line) and ERA5 (pink line) daily precipitation (mm/day) averaged over the mid-lower reaches of the Yangtze river (100°–125°E and 27°–36°N). (c) ERA5 accumulated precipitation anomalies (shading, mm) in June and July 2020 relative to the 1979–2019 climatology (contours, mm) for this time of the year. The black box highlights the Meiyu-Baiu region (110°–140°E and 27°–37°N). The cyan curve denotes the Yangtze River in panel a, c and h. (d) Time series of ERA5 daily precipitation (mm/day) averaged over the Meiyu-Baiu region (black box in panel c) for 2020 (black line) and its climatology (blue line) whose ±1 standard deviation (STD) range is shown by the shading. (e) Arctic SIC in June and July 2020 (shading, %) from ERA5. The red (yellow) curve denotes the 20% SIC contour for 2020 (climatology), and the black box highlights the Siberian coastal region (60°–180°E and 70°–80°N). (f) Time series of ERA5 domain-averaged SIC (orange lines, %) and the fraction of open-water surfaces (purple lines, %) over the Siberian coastal region (black box in panel e) for 2020 (thick lines) and their climatology (thin lines) whose ±1 STD range is shown by the shading. (g) Blocking frequency anomalies (shading, in days) in June and July 2020 relative to the climatology (contours, in days) for this time of the year. The black box highlights the region of East Siberian blocking (90°–180°E and 65°–85°N). (h) Anomalies of the 500-hPa geopotential height (shadings, gpm) and horizontal winds (arrows, m s^{-1}) during the East Siberian blocking days (results for 850-hPa are similar). The black arrows highlight the significant meridional wind anomalies at the 5% level based on a Student's t test.

condition around year 2000 and run for 75 years, including a 25-year spin-up. We further ran two perturbed experiments covering only the period from April 1st to July 31st. In the first perturbation experiment (ARCTIC), SST and SIC were the same as CTL south of 60°N, but north of 60°N they were fixed to the 1995–2005 climatology for April and to those of 2020 from May to July, because the Arctic SIC anomalies became large

only after early May in 2020 (not shown). The other perturbation experiment (GLOBAL) is the same as ARCTIC except it used the 2020 SST and SIC over the globe from May to July. We performed 20 ensemble simulations with slightly different initial conditions for each perturbation experiment and used the ensemble mean to reduce internal variabilities. The GLOBAL-minus-CTL (ARCTIC-minus-CTL) differences represent the atmospheric response to global (Arctic) SST and SIC anomalies in late spring-early summer of 2020. Such SST/SIC-forced atmospheric general circulation model (AGCM) simulations have been widely used to study atmospheric response to sea-ice changes (e.g., Mori et al., 2014); however, this setup cuts off air-ocean-ice interactions and likely results in muted response as the fixed SST/SIC will have a dampening effect on the atmospheric response to perturbations. Nevertheless, these experiments may provide qualitative results for the atmospheric responses to 2020 anomaly SST/SIC conditions, although in reality these surface and atmospheric conditions concur together.

3. Results

3.1. Influence of Excessive East Siberian Blocking on Meiyu-Baiu Rainfall in 2020

In June–July 2020, accumulative rainfall averaged over the Meiyu-Baiu region (black box in Figure 1c) is 412 mm (69%) above normal (Figure 1c). Its temporal evolution shows 8–15 day variations (Figure 1d), implying the effect of atmospheric low-frequency variability such as atmospheric blocking. Meanwhile, Arctic SIC is greatly reduced along the Siberian coast, and more open-water surfaces appeared (Figures 1e and 1f). Overlying the Siberian coast, blocking frequency greatly increased (Figure 1g). These blockings are located at higher latitudes than the Okhotsk Sea blockings that were previously considered as a cause of enhanced Meiyu rainfall (e.g., Park & Ahn, 2014; Wang, 1992). The composites of the blocking days (Figure 1h) over the East Siberian region (black box in Figure 1e) show a large-scale anticyclone that affects the Meiyu-Baiu region (Figure 1f). The anomalous northerlies converge with the anomalous southerlies over the Meiyu-Baiu region, favoring frontogenesis of Meiyu-Baiu front.

The seasonal northward march of the 2020 Meiyu-Baiu rain belt exceeds the climatology before June 20th but lags the climatology during most of the period from June 20th–July 20th (Figure 2a). The intensity and position anomalies of the 2020 Meiyu-Baiu rain belt are significantly correlated with Z500 height anomalies over the East Siberian blocking region, with positive Z500 anomalies associated with southern positions and more Meiyu-Baiu rainfall (Figure 2b). The warm airmass usually advances northward steadily from June to July, but in 2020 its northward migration was interrupted by three cold airmass outbreaks in late June, early July, and mid-July (Figure 2c). These cold airmass outbreaks correspond to three East Siberian blockings (pink shading in Figure 2b) except for the one in mid-June, associated with which the anomalous northerlies were seen over the Meiyu-Baiu region in blocking's early development stage (Figure 2b) but shifted eastward over the western Pacific as the blocking's zonal size became large in its mature stage (not shown). During the blocking periods in June–July 2020, the blocking anticyclone induces anomalous northerly winds on its eastern side (Figure 1h) that pushes the Meiyu-Baiu rainbelt southward (Figures 2b and 2c). As a result, the northern part of the Meiyu-Baiu region is occupied by northerly winds and cold air (Figure 2c). The temperature in its northern part decreases, but the meridional temperature gradient increases across the front (Figure 2c). Thus, the East Siberian blockings obstructed the northward movement of the 2020 Meiyu-Baiu rainfall and increased the thermal contrast across the front. These results are consistent with previous studies (e.g., Chen et al., 2007; Li et al., 2001; Ninomiya & Shibagaki, 2007), which suggested that Asian high-latitude blocking favors the Meiyu-Baiu frontogenesis and a persistent Meiyu-Baiu front.

3.2. The Link Between Low Arctic Sea Ice and East Siberian Blocking

The positive height anomalies over the East Siberian blocking region persisted for more than one month (Figure 2c), which is much longer than a normal atmospheric signal, implying a lower-boundary forcing of such a long-lived atmospheric anomaly. In June–July 2020, an unusual narrow warm belt occurred along the Siberian coast (Figure 3a), together with reduced sea ice cover over the marginal sea off Siberia in the late spring-early summer (Figure 1c). Based on ERA5, absorbed shortwave radiation, upward longwave radiation, surface sensible and latent heat fluxes averaged over the Siberian coastal ocean (black box in Figure 3a) in June–July 2020 were, respectively, 13.1%, 2.1%, 19.9%, and 11.8% above normal, due to

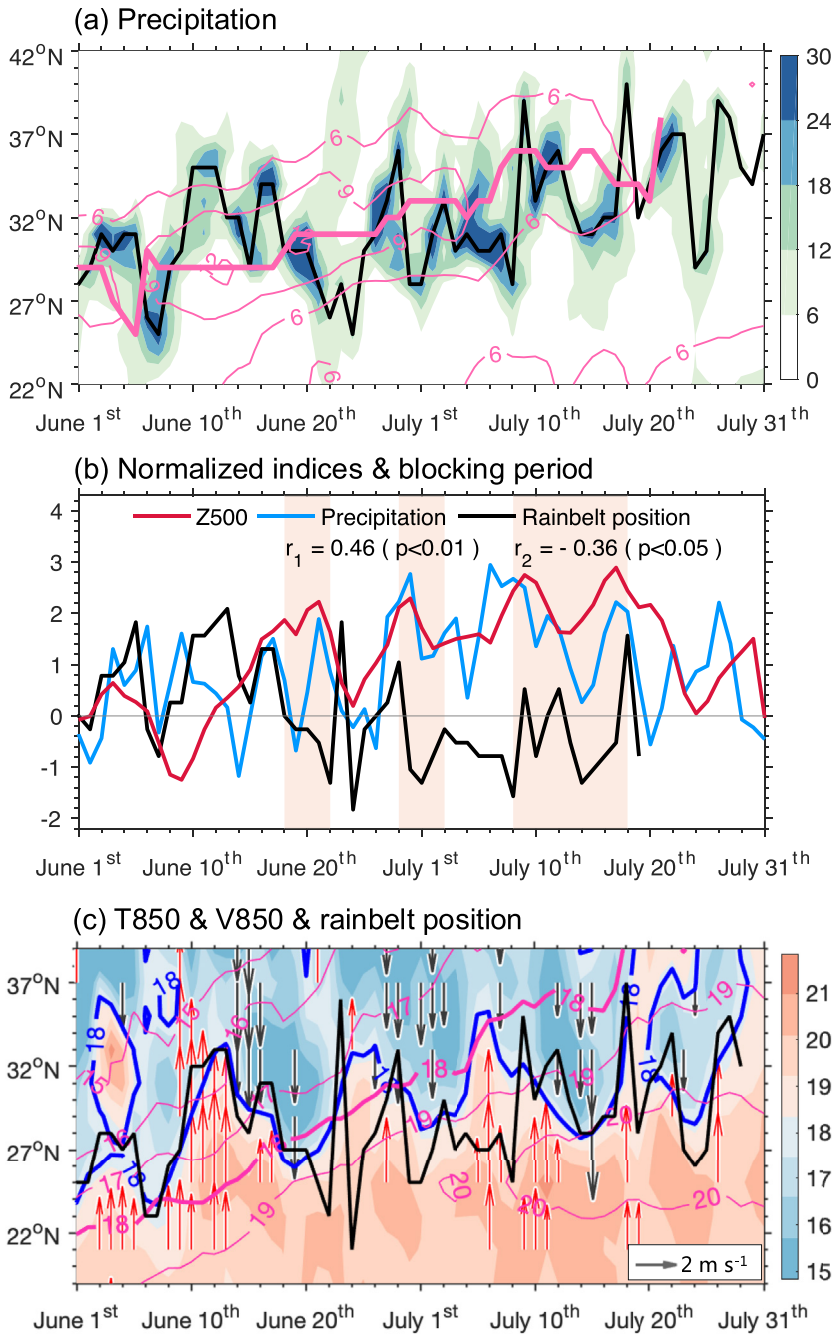

Figure 2. Daily evolutions of the Meiyu-Baiu rain belt and the associated atmospheric circulation. (a) Time-latitude distribution of ERA5 daily precipitation (shading, mm/day) averaged over the Meiyu-Baiu region (black box in Figure 1a) in 2020 and its climatology (contours, mm). The black line denotes the latitude position of the maximum daily precipitation in 2020 and the pink line denotes its climatology. (b) Normalized time series (in units of STD) of daily Z500 (red line) averaged over the East Siberian blocking region (black box in Figure 1g), precipitation averaged over the Meiyu-Baiu region (blue line), latitude position of the daily maximum Meiyu-Baiu precipitation (black line, obtained from the black line in panel a). Pink shadings denote the days with instantaneous East Siberian blockings. The correlation coefficients ($r_1 = 0.46$ and $r_2 = -0.36$) are for Z500 versus precipitation and Z500 versus rain belt position, respectively. (c) Time-latitude distribution of ERA5 daily 850-hPa air temperature (T850) averaged over the Meiyu-Baiu longitude sector in 2020 (shading, °C) with the 18°C contour highlighted by the blue line, and its climatology (contours, °C) with the 18°C contour highlighted by thick pink line. The gray (red) arrow denotes 850-hPa southward (northward) wind anomaly significant at the 10% level, and the black line is same as panel a.

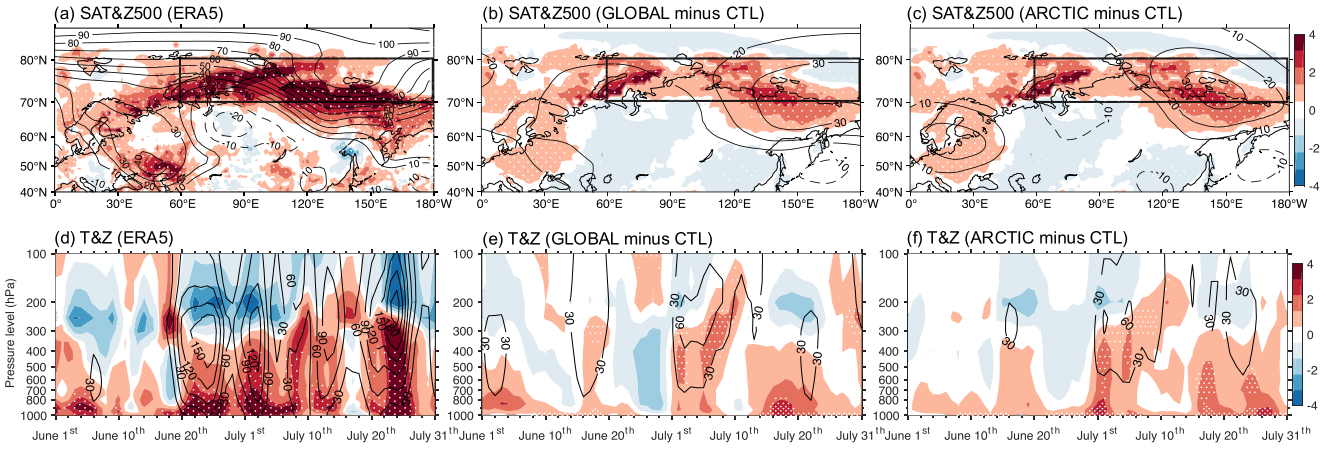

Figure 3. Temperature and height anomalies. (a) ERA5 surface air temperature (SAT, shading, °C) and Z500 (contours, gpm) anomalies during June–July 2020, and the CAM6-simulated (b) GLOBAL-minus-CTL and (c) ARCTIC-minus-CTL differences of SAT (shading, °C) and Z500 (contours, gpm) averaged from June to July over the Eurasian region. The black box highlights the Siberian coastal region (60°–180°E and 70°–80°N, same as the black box in Figure 1c). Pressure-time cross-sections of ERA5 (d) air temperature (T, shading, °C) and geopotential height (Z, contours, gpm) anomalies and (e) GLOBAL-minus-CTL and (f) ARCTIC-minus-CTL T (shading, °C) and Z (contours, gpm) differences zonally-averaged over the Siberian coastal region (black box in panel a–c). Stippled regions are significant at the 5% level for air temperatures based on a Student's t test.

increased open-water surfaces (Figure 1d), which are a heat source to the atmosphere during cold seasons (Dai et al., 2019). This indicates that increased open-water surfaces in June–July 2020 absorbed more solar radiation and released more heat to warm the atmosphere, contributing to the surface air warming along the Siberian coast (Figure 3a). This warming extends into the mid-upper troposphere from late June to late July, corresponding to positive height anomalies in the mid-upper troposphere (Figure 3d).

The CAM6 simulations provide a partial estimate of atmospheric response to the SIC and SST anomalies. The GLOBAL-minus-CTL differences for surface air temperature (SAT) and Z500 over mid-high latitude Eurasia resemble the ERA5 results with reduced amplitudes (Figures 3a and 3b) and are similar to the ARCTIC-minus-CTL differences (Figure 3c). This indicates that the Siberian coastal warming and East Siberian blockings can be partially attributed to the Arctic SIC/SST anomalies in the late spring-early summer of 2020. Similar to the ERA5 results, the near-surface warming precedes the deep tropospheric warming and positive height anomalies in the model simulations (Figures 3e and 3f), suggesting that they are originated from surface heating.

Associated with the Siberian coastal warming, the meridional gradient of lower tropospheric temperatures (dT/dy) decreases south of the Siberian coast (Figures 4a–4c). A smaller dT/dy would weaken the zonal wind according to the thermal wind relation (Figures 4d–4f) and decrease regional baroclinicity and eddy momentum flux convergence (Figures 4g–4i). The latter would decrease the eddy-driven component of the subpolar jet (Figures 4d–4i) south of the Siberian coast. Previous studies suggest that a weak zonal wind is a pre-condition for frequent and persistent blockings (e.g., Luo et al., 2019). Thus, the low sea ice cover along the Siberian coast contributes to the warming and high pressure over the region, reduces dT/dy and the zonal wind south of it, and thus favors the occurrence and maintenance of East Siberian blockings. This is in line with previous studies that suggested summer warming along Arctic coasts can modulate the subpolar jet and large-scale waves (e.g., Coumou et al., 2018; Knudsen et al., 2015; Petrie et al., 2015).

The ARCTIC-minus-CTL precipitation differences (Figure 5a) averaged from June to July reasonably capture the observed Meiyu-Baiu rainfall anomalies (Figure 1a), and the precipitation differences (Figures 5b and 5c) last into July, which is consistent with the ERA5 results (Figure 2a). However, the GLOBAL-minus-CTL and ARCTIC-minus-CTL precipitation differences only reproduce, respectively, 23.14% and 27.57% of the ERA5 Meiyu-Baiu rainfall anomalies in June–July 2020 (2.98 mm/day). This implies that our atmospheric experiments without two-way air-ocean-ice interactions may underestimate the atmosphere responses to sea-ice and SST anomalies.

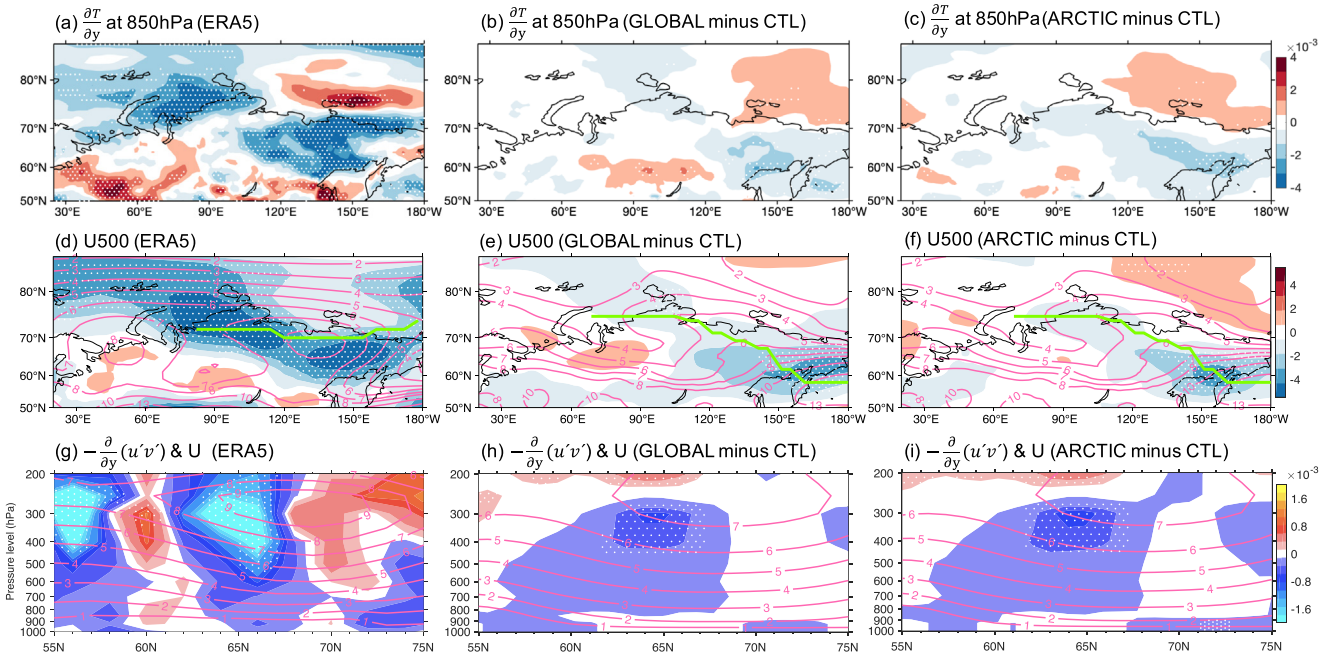

Figure 4. Temperature gradient and wind anomalies. (a) ERA5 meridional gradients of 850-hPa air temperature anomalies ($\frac{\partial T}{\partial y}$, °C km^{-1}) averaged over June and July 2020, and (b) GLOBAL-minus-CTL and (c) ARCTIC-minus-CTL differences of the same temperature gradient (°C km^{-1}) averaged over June and July. (d) ERA5 500-hPa zonal wind (U500) anomalies (shading, m s^{-1}) averaged over June and July 2020 and its climatology (contours, m s^{-1}) for this time of the year. (e) GLOBAL-minus-CTL and (f) ARCTIC-minus-CTL U500 differences (shading, m s^{-1}) averaged over June and July and the U500 climatology in CTL for this time of the year (contours, m s^{-1}). The thick green line denotes the approximate position of the subpolar jet axis over Asia. Pressure-latitude cross-sections of (g) $-\frac{\partial}{\partial y}(u'v')$ anomalies (shading, m s^{-2}) and zonal wind climatology (contours, m s^{-1}) from ERA5, and (h) GLOBAL-minus-CTL and (i) ARCTIC-minus-CTL differences of $-\frac{\partial}{\partial y}(u'v')$ (shading, m s^{-2}) and zonal wind climatology in CTL (contours, m s^{-1}) for June and July and over 60°–180°E, where u' (v') denotes 8-day high-pass-filtered daily zonal (meridional) wind, $-\frac{\partial}{\partial y}(u'v')$ represents the meridional convergence of the eddy momentum flux. Low $-\frac{\partial}{\partial y}(u'v')$ denotes less energy being transferred from eddies to mean flow. Stippled regions are significant at the 5% level.

4. Summary and Discussion

In this study, we have analyzed observations and ERA5 data and performed atmospheric model simulations to examine the causes of the 2020 extreme Meiyu-Baiu rainfall. It is found that the low sea-ice cover in late spring-early summer along the Siberian coast contributed to the surface and tropospheric warming. The zonal-oriented warming along the Siberian coast decreases the meridional temperature gradient, eddy momentum flux convergence, and zonal wind south of the Siberian coast. These conditions favor the East Siberian blockings, which caused three cold air outbreaks into the Meiyu-Baiu region from mid-June to

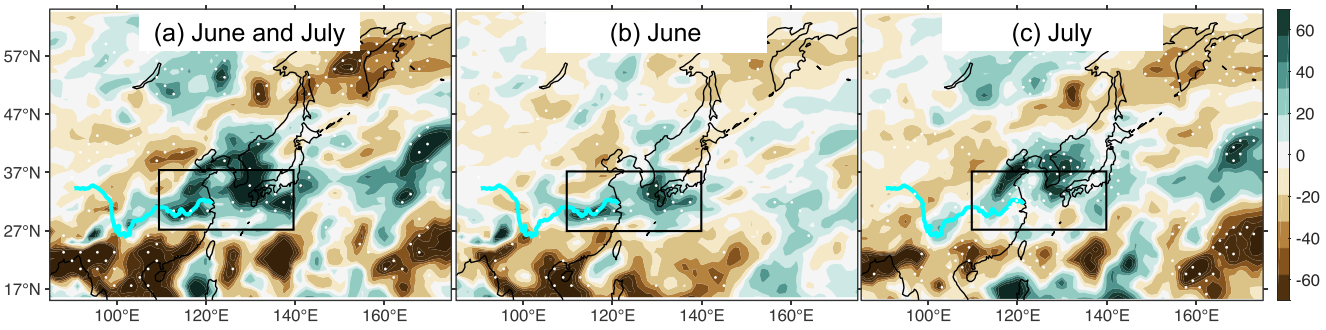

Figure 5. ARCTIC-minus-CTL precipitation differences (mm/day) for (a) June–July mean, (b) June, and (c) July. Stippling indicates the difference is significant at the 5% level. The black box highlights the Meiyu-Baiu region. GLOBAL-minus-CTL precipitation differences are similar (not shown).

mid-July 2020. These southward intrusions of cold air stopped the seasonal northward march of the Meiyu-Baiu front and increased the thermal contrast across the front, causing intense and prolonged Meiyu rainfall in June–July 2020.

Our findings suggest an important role of Arctic sea-ice loss for the record-breaking Meiyu rainfall in June–July 2020. This provides a contrasting and complementary explanation of the 2020 Meiyu rainfall anomaly in comparison with recent studies by Takaya et al. (2020) and Zhou et al. (2021), who suggested a significant role of the warm Indian Ocean, which can help explain the enhanced Meiyu rainfall in June but not July of 2020 (Zhou et al., 2021). The record-breaking low sea-ice cover during the late spring-early summer of 2020 likely resulted from natural variations and long-term sea-ice loss. Our results suggest that such sea-ice anomalies under current warming climate can affect local atmospheric temperatures and atmospheric blockings, and therefore influence the Meiyu-Baiu rainfall. As atmospheric greenhouse gases continue to increase, Arctic sea ice will decrease further, more warm ocean water surfaces will be exposed in Arctic winter, and this will result in enhanced Arctic warming (Dai et al., 2019). As late spring-early summer sea ice decreases along the Siberian coast, sea-ice's year-to-year variations may change and disappear eventually as sea ice melts away completely (Dai and Deng, 2021). How the long-term sea-ice loss and Arctic warming affect East Siberian blocking and the Meiyu-Baiu front requires further investigation. Lastly, although our experiments properly simulate the enhanced 2020 Meiyu-Baiu rainfall and provide qualitatively consistent results, quantitative estimates of the contribution from the Arctic anomaly SST/SIC conditions require improved experimental designs.

Data Availability Statement

The ERA5 reanalysis data is available via https://cds.climate.copernicus.eu/cdsapp#!/dataset/reanalysis-era5-single-levels?tab=form. The model simulation data analyzed in this study and the raingauge measurement are available through https://doi.org/10.4121/13683703.v1 and https://doi.org/10.4121/13685476.v1, respectively.

Acknowledgments
The authors thank two anonymous reviewers for constructive comments. X. Chen was supported by the China Postdoctoral Science Foundation (2020M681153 and BX20200087). A. Dai was supported by the National Science Foundation (grant nos. AGS-2015780 and OISE-1743738) and the U.S. National Oceanic and Atmospheric Administration (grant no. NA18OAR4310425). Z. Wen acknowledges the support of National Sciences Foundation of China Grants (42030601).

References

Chen, G. T.-J., Wang, C.-C., & Wang, A.-H. (2007). A case study of subtropical frontogenesis during a blocking event. *Monthly Weather Review*, *135*(7), 2588–2609. https://doi.org/10.1175/MWR3412.1

Chen, X., Luo, D., Wu, Y., Dunn-Sigouin, E., & Lu, J. (2020). Nonlinear response of atmospheric blocking to early winter Barents-Kara Seas warming: An idealized model study. *Journal of Climate*, *34*(6), 2367–2383. https://doi.org/10.1175/JCLI-D-19-0720.1

Chen, Y., & Zhai, P. (2014). Two types of typical circulation pattern for persistent extreme precipitation in Central-Eastern China. *Quarterly Journal of the Royal Meteorological Society*, *140*(682), 1467–1478. https://doi.org/10.1002/qj.2231

Coumou, D., Di Capua, G., Vavrus, S., Wang, L., & Wang, S. (2018). The influence of Arctic amplification on mid-latitude summer circulation. *Nature Communications*, *9*, 2949. https://doi.org/10.1038/s41467-018-05256-8

Dai, A., & Deng, J. (2021). Arctic amplification weakens the variability of daily temperatures over northern middle-high latitudes. *Journal of Climate*, *34*, 2591–2609. https://doi.org/10.1175/JCLI-D-20-0514.1

Dai, A., Luo, D., Song, M., & Liu, J. (2019). Arctic amplification is caused by sea-ice loss under increasing CO2. *Nature Communications*, *10*, 121. https://doi.org/10.1038/s41467-018-07954-9

Dai, A., & Song, M. (2020). Little influence of Arctic amplification on mid-latitude climate. *Nature Climate Change*, *10*, 231–237. https://doi.org/10.1038/s41558-020-0694-3

Danabasoglu, G., Lamarque, J. F., Bacmeister, J., Bailey, D. A., DuVivier, A. K., Edwards, J., et al. (2020). The community earth system model Version 2 (CESM2). *Journal of Advances in Modeling Earth Systems*,*12*, e2019MS001916. https://doi.org/10.1029/2019MS001916

Ding, Y. (1991). *Monsoon over China* (p. 419). Kluwer Academic Pub.

Dunn-Sigouin, E., Son, S.-W., & Lin, H. (2013). Evaluation of Northern Hemisphere blocking climatology in the global environment multiscale model. *Monthly Weather Review*, *141*(2), 707–727. https://doi.org/10.1175/MWR-D-12-00134.1

Hersbach, H., Bell, B., Berrisford, P., Hirahara, S., Horányi, A., Muñoz-Sabater, J., et al. (2020). The ERA5 global reanalysis. *Quarterly Journal of the Royal Meteorological Society*, *146*(730), 1999–2049. https://doi.org/10.1002/qj.3803

Huang, R., & Wu, Y. (1989). The influence of ENSO on the summer climate change in China and its mechanism. *Advances in Atmospheric Sciences*, *6*, 21–32. https://doi.org/10.1007/BF02656915

Knudsen, E. M., Orsolini, Y. J., Furevik, T., & Hodges, K. I. (2015). Observed anomalous atmospheric patterns in summers of unusual Arctic sea ice melt. *Journal of Geophysical Research - D: Atmospheres*, *120*(7), 2595–2611. https://doi.org/10.1002/2014JD022608

Kosaka, Y., Xie, S.-P., Lau, N.-C., & Vecchi, G. A. (2013). Origin of seasonal predictability for summer climate over the Northwestern Pacific. *Proceedings of the National Academy of Sciences*, *110*(19), 7574–7579. https://doi.org/10.1073/pnas.1215582110

Li, S., Ji, L., Lin, W., & Ni, Y. (2001). The maintenance of the blocking over the Ural Mountains during the second Meiyu period in the summer of 1998. *Advances in Atmospheric Sciences*, *18*, 87–105. https://doi.org/10.1007/s00376-001-0006-4

Li, Y., Deng, Y., Yang, S., & Zhang, H. (2018). Multi-scale temporospatial variability of the east Asian Meiyu-Baiu fronts: characterization with a suite of new objective indices. *Climate Dynamics*, *51*(5), 1659–1670. https://doi.org/10.1007/s00382-017-3975-4

Liu, B., Yan, Y., Zhu, C., Ma, S., & Li, J. (2020). Record-breaking Meiyu rainfall around the Yangtze River in 2020 regulated by the subseasonal phase transition of the north atlantic oscillation. *Geophysical Research Letters*, *47*(2). e2020GL090342. https://doi.org/10.1029/2020GL090342

Luo, D., Chen, X., Overland, J., Simmonds, I., Wu, Y., & Zhang, P. (2019). Weakened potential vorticity barrier linked to recent winter Arctic Sea ice loss and midlatitude cold extremes. *Journal of Climate*, *32*(14), 4235–4261. https://doi.org/10.1175/JCLI-D-18-0449.1

Luo, D., & Zhang, W. (2020). A nonlinear multiscale theory of atmospheric blocking: Dynamical and thermodynamic effects of meridional potential vorticity gradient. *Journal of the Atmospheric Sciences*, *77*(7), 2471–2500. https://doi.org/10.1175/JAS-D-20-0004.1

Mori, M., Watanabe, M., Shiogama, H., Inoue, J., & Kimoto, M. (2014). Robust Arctic sea-ice influence on the frequent Eurasian cold winters in past decades. *Nature Geoscience*, *7*, 869–873. https://doi.org/10.1038/ngeo2277

Ninomiya, K., & Shibagaki, Y. (2007). Multi-scale features of the Meiyu-Baiu front and associated precipitation systems. *Journal of Meteorological Society of Japan*, *85B*, 103–122. https://doi.org/10.2151/jmsj.85B.103

NSIDC. (2020). *Siberian downward slide*. http://nsidc.org/arcticseaicenews/2020/07/siberian-downward-slide/

Overland, J. E., & Wang, M. (2020). The 2020 Siberian heat wave. *International Journal of Climatology*, *41*, E2341–E2346. https://doi.org/10.1002/joc.6850

Pan, Y., Shen, Y., Yu, J., & Xiong, A. (2015). An experiment of high-resolution gauge-radar-satellite combined precipitation retrieval based on the Bayesian merging method. *Acta Meteorologica Sinica*, *73*, 177–186.

Park, Y. J., & Ahn, J. B. (2014). Characteristics of atmospheric circulation over East Asia associated with summer blocking. *Journal of Geophysical Research - D: Atmospheres*, *119*(2), 726–738. https://doi.org/10.1002/2013JD020688

Petrie, R. E., Shaffrey, L. C., & Sutton, R. T. (2015). Atmospheric response in summer linked to recent Arctic sea ice loss. *Quarterly Journal of the Royal Meteorological Society*, *141*(691), 2070–2076. https://doi.org/10.1002/qj.2502

Ren, X., Yang, X.-Q., & Sun, X. (2013). Zonal oscillation of western pacific subtropical high and subseasonal SST variations during yangtze persistent heavy rainfall events. *Journal of Climate*, *26*(22), 8929–8946. https://doi.org/10.1175/JCLI-D-12-00861.1

Ruggieri, P., Buizza, R., & Visconti, G. (2016). On the link between Barents-Kara sea ice variability and European blocking. *Journal of Geophysical Research - D: Atmospheres*, *121*(10), 5664–5679. https://doi.org/10.1002/2015JD024021

Si, D., Ding, Y., & Liu, Y. (2009). Decadal northward shift of the Meiyu belt and the possible cause. *Science Bulletin*, *54*, 4742–4748. https://doi.org/10.1007/s11434-009-0385-y

Takaya, Y., Ishikawa, I., Kobayashi, C., Endo, H., & Ose, T. (2020). Enhanced Meiyu-Baiu rainfall in early summer 2020: Aftermath of the 2019 super IOD event. *Geophysical Research Letters*, *47*(22). e2020GL090671. https://doi.org/10.1029/2020GL090671

Tao, S., & Chen, L. (1987). A review of recent research on the East Asia summer monsoon over China In *Monsoon meteorology* (pp. 50–92). Oxford Univ. Press.

Wang, Y. (1992). Effects of blocking anticyclones in Eurasia in the rainy season (Meiyu/Baiu season). *Journal of the Meteorological Society of Japan*, *70*(5), 929–951. https://doi.org/10.2151/jmsj1965.70.592910.2151/jmsj1965.70.5_929

WMO. (2020). *WMO El Niño/La niña update*. http://www.wmo.int/pages/prog/wcp/wcasp/enso_update_latest.html

Wu, R., & Hu, Z.-Z., Kirtman, B. P. 2003). Evolution of ENSO-related rainfall anomalies in East Asia. *Journal of Climate*, *16*(22), 3742–3758. https://doi.org/10.1175/15200442(2003)016<3742:EOERAI>2.0.CO;2

WWA. (2020). *WWA press release, "Prolonged Siberian heat of 2020"*. https://www.worldweatherattribution.org/wp-content/uploads/WWA-Prolonged-heat-Siberia-2020.pdf

Xiao, Z., & Duan, A. (2016). Impacts of tibetan plateau snow cover on the interannual variability of the East Asian summer monsoon. *Journal of Climate*, *29*(23), 8495–8514. https://doi.org/10.1175/JCLID160029110.1175/jcli-d-16-0029.1

Yao, Y., Luo, D., Dai, A., & Simmonds, I. (2017). Increased quasi stationarity and persistence of winter ural blocking and eurasian extreme cold events in response to arctic warming. Part I: Insights from observational analyses. *Journal of Climate*, *30*(10), 3549–3568. https://doi.org/10.1175/JCLI-D-16-0261.1

Yim, S.-Y., Jhun, J.-G., Lu, R., & Wang, B. (2010). Two distinct patterns of spring Eurasian snow cover anomaly and their impacts on the East Asian summer monsoon. *Journal of Geophysical Research*, *115*, D22113. https://doi.org/10.1029/2010JD013996

Zhang, H., Wen, Z., Wu, R., Chen, Z., & Guo, Y. (2017). Inter-decadal changes in the East Asian summer monsoon and associations with sea surface temperature anomaly in the South Indian Ocean. *Climate Dynamics*, *48*(3–4), 1125–1139. https://doi.org/10.1007/s00382-016-3131-6

Zhang, P., Wu, Z., & Jin, R. (2021). How can the winter North Atlantic Oscillation influence the early summer precipitation in Northeast Asia: Effect of the Arctic sea ice. *Climate Dynamics*, *56*(5), 1989–2005. https://doi.org/10.1007/s00382-020-05570-2

Zhou, Z.-Q., Xie, S.-P., & Zhang, R. (2021). Historic Yangtze flooding of 2020 tied to extreme Indian Ocean conditions. *Proceedings of the National Academy of Sciences of the United States of America*, *118*(12), e2022255118. https://doi.org/10.1073/pnas.2022255118

Zhu, C., Nakazawa, T., Li, J., & Chen, L. (2003). The 30-60 day intraseasonal oscillation over the western North Pacific Ocean and its impacts on summer flooding in China during 1998. *Geophysical Research Letters*, *30*(18), 1952. https://doi.org/10.1029/2003GL017817

Zhu, Y., Wang, H., Ma, J., Wang, T., & Sun, J. (2015). Contribution of the phase transition of Pacific decadal oscillation to the late 1990s' shift in East China summer rainfall. *Journal of Geophysical Research - D: Atmospheres*, *120*(17), 8817–8827. https://doi.org/10.1002/2015JD023545